High-performance inverted planar perovskite solar cells using pristine fullerene mixture as electron-transport layer

Chongyang Xu,[a] Zhihai Liu,*[b] and Eun-Cheol Lee*[a]

[a]Department of Nano-Physics, Gachon University, Seongnam, 13120, Republic of Korea

[b]Department of Bio-Nano Technology, Gachon University, Seongnam, 13120, Republic of Korea

*Corresponding authors. E-mail addresses: zhliu@gachon.ac.kr, eclee@gachon.ac.kr

ABSTRACT: Fullerene derivatives are widely used as efficient electron-transport materials for inverted perovskite solar cells (PSCs). Among them, phenyl-C_x-butyric acid methyl ester (PC_xBM; x = 61 or 71) is the most frequently used because of its high solubility and solution processability. However, chemical modification of original fullerenes (C_{60} or C_{70}) will decrease the charge mobility, which is detrimental to the performance of PSCs. Moreover, the high cost of fullerene derivatives (such as PCBMs) is an obstacle hindering the commercialization of the PSCs. In this study, we developed a pristine fullerene mixture (FM) composed of C_{60} and C_{70} as an electron-transport layer (ETL). Because of the increased configurational entropy, the solubility of the C_{60} and C_{70} mixture was significantly improved to 52.9 g L^{-1} (in dichlorobenzene), which may reduce the speed of crystallization of the FM during the spin-coating process, in which the organic solvent is evaporated. With this FM-based ETL, PSCs exhibited an average power-conversion efficiency (PCE) of 16.9%, which was higher than that (15.2%) of $PC_{61}BM$-based ones. Additionally, the FM-based ETL exhibited greater hydrophobicity than $PC_{61}BM$, which led to better moisture tolerance. As a result, the long-term stability of the FM-based PSCs was improved significantly, with reduced PCE degradation (from 26% to 15%) after 150 h under ambient conditions.

Introduction

Since the use of perovskite in sensitized solar cells was first reported by Miyasaka et al.,[1] organic–inorganic hybrid organometal halide perovskite solar cells (PSCs) have been intensively studied, with their power-conversion efficiency (PCE) rapidly exceeding 23%.[2-4] PSCs are regarded as one of the most promising candidates for next-generation photovoltaic technology owing to their advantages of high light-absorption coefficients, light weight, and simple fabrication processes.[5-11] Despite these advantages, PSCs present problems, such as the short device lifetime, high fabrication cost, low environmental reliability, poor reproducibility, and toxicity of the component elements, which need to be solved before commercialization.[12]

PSCs can be classified as conventional-structure, in which a transparent indium-tin-oxide (ITO) or fluorine-doped tin-oxide (FTO) electrode is used as the cathode, and inverted-structure, in which ITO or FTO is used as the anode.[13-20] In inverted PSCs, poly(3,4-ethylenedioxylenethiophene):poly(styrene sulfonate) and poly(bis(4-phenyl)(2,4,6-trimethylphenyl)amine) (PTAA) are typically used as hole-transport layers (HTLs) and are coated on top of the anode.[21-23] Fullerene derivatives, such as phenyl-C_x-butyric acid methyl esters (PCBMs; x = 61 or 71), are widely used as electron-transport layers (ETLs) owing to their excellent solubility, which satisfies the requirement of solution processability.[24-26] However, attaching exohedral moieties to the pristine fullerene cage will sacrifice the original high electron mobility and lead to an increased material costs.[27-29] In contrast, pristine C_{60} and C_{70} are inexpensive and

exhibit better electron mobility than PCBMs.[30] However, their poor solubility in organic solvents makes it difficult to form a continuous and homogeneous film, owing to the strong tendency of crystallization during the spin-coating process.[30, 31] Nevertheless, it remains unclear which material (C_{60} or $PC_{61}BM$) can lead to a higher PCE for PSCs. For example, Jeng et al. firstly compared the performance of PSCs employing C_{60} and $PC_{61}BM$ as ETLs via an evaporation method and found that the C_{60}-based PSCs exhibited a lower PCE (1.6%) than that (2.4%) of $PC_{61}BM$-based ones.[32] However, Liang and coworkers found that using C_{60} as ETL in a PSC yielded a higher PCE (15.44%) than using $PC_{61}BM$ (13.37%).[33] On the other hand, evaporation of a thin C_{60} layer onto $PC_{61}BM$ achieve higher PCEs than those of PSCs only using $PC_{61}BM$ or C_{60} as ETL.[34, 35] However, the evaporation method is energy-consuming and equipment-demanding, and the mechanism underlying the efficiency improvement provided by the C_{60}/PCBM bilayer is unclear.[36, 37] Mendaza et al. used mixtures of fullerenes (C_{60} and C_{70}) as the electron acceptor in organic transistors and solar cells, resolving the issues related to the photoelectric performance and cost-effectiveness.[30] In their study, the fullerene mixture (FM)-based devices exhibited comparable performance to $PC_{61}BM$-based devices, because a proper ratio of the FM can obviously enhance the solubility in an organic solvent and thus satisfy the requirement of the solution process.[30] Furthermore, the employment of the FM significantly reduced the energy cost (from 90 to 8 GJ kg^{-1}), which includes the purification of pristine fullerene and the synthesis of PCBM from fullerene.[38] In order to reduce the fabrication cost of

4

PSCs for commercialization, the FM is a good candidate for replacing conventional PCBMs as the ETL. Considering the low-cost requirement of PSC commercialization, it is very important to investigate FM as ETL in PSC fabrications. Recently, Lin et al. reported the use of an FM (9:1 mixture of C_{60} and C_{70}) as an ETL, which resulted in a high PCE of 16.7% for conventional-structure PSCs.[39] In that work, the authors mainly focused on the fabrication of conventional-structure PSCs, and the use of the same FM in the inverted structure led to a PCE (15.2%) lower than that obtained using C_{60} (15.8%). However, in the case of utilizing FM as the ETL, inverted structures have a clear advantage over conventional structures: in conventional structures, the ETL might be damaged by a solvent such as *N,N*-dimethylformamide (DMF) in the perovskite precursor, whereas no such damage occurs in inverted structures. In the previous study, a fixed blending ratio (9:1) of C_{60} and C_{70} and a fixed fullerene concentration of 20 mg mL^{-1} in the solvent were used for the inverted structures.[39] However, a systematic study of different blending ratios and fullerene concentration in the solvent is required for inverted-structure devices.

In the present study, we focused on the inverted-type PSCs and significantly improved the solubility of pristine fullerene by dissolving a mixture of C_{60} and C_{70} into organic solvents and optimizing the blending ratio. The high solubility of the C_{60} and C_{70} mixture in ortho-dichlorobenzene (*o*-DCB, 52.9 g L^{-1}) ensured the formation of a homogeneous film in the spin-coating process.[40, 41] Consequently, PSCs based on the FM exhibited a high PCE of 16.9% (on average). This PCE was 11.2% higher than that

of PSCs using PC$_{61}$BM (15.2%), mainly because of the enhanced short-circuit current density (J_{sc}) and fill factor (FF). Additionally, the use of the FM as the ETL improved the long-term stability of the devices compared with the case of using PC$_{61}$BM; the PCE (normalized to the initial value) after 150 h under ambient conditions increased from 74% to 85%. This is because of the high hydrophobicity of the FM layer, which efficiently blocked moisture from the environment. Thus, the proposed approach is effective for improving the performance and reducing the cost of PSCs, both of which are important for commercialization.

Experimental

Chemicals and reagents

Lead iodide (PbI$_2$), cesium iodide (CsI), isopropanol (IPA), chlorobenzene (CB), *o*-DCB, toluene, dimethylsulfoxide (anhydrous, 99.8%), DMF, acetonitrile, Li-bis(trifluoromethanesulfonyl)imide (Li salt), and 4-*tert*-butylpyridine (tBP) were purchased from Sigma–Aldrich (USA). PC$_{61}$BM, C$_{60}$, and C$_{70}$ were purchased from Nano-C Inc. (USA). Methylammonium iodide (MAI) and 2,9-dimethyl-4,7-diphenyl-1,10-phenanthroline (BCP) were purchased from Xi'an Polymer Light Technology Corp. (China). Patterned ITO glasses and PTAA were purchased from Ying Kou You Xuan Trade Co., Ltd. (China) and EM Index (Korea), respectively.

FM solubility measurements

C_{60} and C_{70} were dissolved in o-DCB, CB, and toluene with various weight ratios (ranging from 1:0 to 0:1) at 25 °C under continuous stirring for 12 h. The solubility of C_{60} and C_{70} in each solvent was determined by filtering and weighing the sediment, which was completely dried under vacuum conditions for 3 h.

Device fabrication

The PSCs were fabricated on the ITO glasses with a configuration of ITO/PTAA/perovskite/ETL ($PC_{61}BM$ or C_{60}:C_{70})/BCP/Ag, as shown in Fig. 1a. The ITO-coated glass substrates were cleaned sequentially with detergent, deionized water, and IPA and treated in an ultraviolet (UV)–ozone cleaner for 20 min. A PTAA solution was prepared by dissolving 10 mg of PTAA in 1 mL of toluene with the following additives: 7.5 µL of a Li-salt solution in acetonitrile (170 mg mL^{-1}) and 4 µL of tBP. The PTAA layer was formed by spin-coating the solution onto ITO glass at 3000 rpm for 30 s, followed by thermal annealing at 110 °C for 10 min. The perovskite precursor solution was prepared by dissolving CsI, MAI, and PbI_2 (molar ratio of 0.05:0.95:1) in anhydrous DMF to obtain a stoichiometric solution with a total concentration of 1.25 M, which was then stirred for 12 h at 60 °C. The $Cs_{0.05}MA_{0.95}PbI_3$ perovskite was formed by spin-coating the precursor solution onto the PTAA-coated samples at 4000 rpm for 30 s in a N_2-filled glove box. During the spin-coating process, 200 µL of CB (anti-solvent) was quickly dropped onto the samples at a delay time of 8 s. The samples were subsequently annealed on a hotplate at 100 °C for 10 min. Next, 50 µL of a

PC$_{61}$BM or FM solution with a concentration of 30.0 mg mL^{-1} was spin-coated at 2000 rpm for 30 s to form the ETL. When the fullerene solubility of the ETL solution was <30.0 mg mL^{-1}, fullerene precipitates were formed in the solution. In this case, the precipitates were filtered out of the solution. Next, 70 μL of a BCP solution (0.5 mg mL^{-1} in IPA) was spin-coated onto the ETL at 4000 rpm. Finally, a 100-nm-thick Ag electrode was coated on top of the samples to form an effective working area of 0.1 cm^2 (defined by a 0.2-cm-wide ITO bar and a 0.5-cm-wide Ag bar) using a thermal evaporator under high vacuum (<6.0 × 10^{-6} Torr).

Characterization

Phase images of the films in air were obtained using atomic force microscopy (AFM, Veeco, USA) in the tapping mode. Top-view and cross-sectional scanning electron microscopy (SEM) images were obtained using a JSM-7500F field-emission scanning electron microscope (JEOL, Japan) at an acceleration voltage of 20 kV. The steady-state photoluminescence (PL) and time-resolved PL (TRPL) spectra were measured using a spectrometer (FLS920, Edinburgh Instruments, UK). The current density–voltage (J–V) characteristics of the PSCs were measured under an irradiation intensity of 100 mW cm^{-2} (AM 1.5). The incident photon-to-electron conversion efficiency (IPCE) was measured using Solar Cell Scan 100 (Zolix, China). The space-charge-limited current (SCLC) of the electron-only device, i.e., ITO/Al/ETL (PC$_{61}$BM or C$_{60}$:C$_{70}$/Al), was measured using a 2400 Source Meter in a dark environment with a

bias voltage of 1 V. Electrochemical impedance spectroscopy (EIS) of the devices was performed in a dark environment using an electrochemical workstation (CH Instruments, USA). UV–visible (UV–vis) absorption spectra were recorded using a UV–vis–NIR 3600 spectrometer (Shimadzu, Japan). X-ray diffraction (XRD) measurements were measured by a Rigaku Smart Lab X-ray diffractometer (Japan) with Cu Kα radiation (λ = 1.5418 Å) at room temperature. The ultraviolet photoelectron spectroscopy (UPS) was acquired with a Kratos Axis Ultra X-ray photoelectron spectroscope (Kratos Analytical, UK).

Results and discussion

As indicated by the chemical structures in Fig. 1b, $PC_{61}BM$ is a derivative of C_{60} and has high solubility in organic solvents compared with pristine fullerenes.[30, 31] This is because the sidechain of $PC_{61}BM$ presents steric hindrance, which affects the solvent molecule distribution in the solvent and thus enhances the solubility.[31] In contrast, pristine C_{60} and C_{70} species form a stable solvation shell in the solvent, leading to poor solubility of C_{60} and C_{70} in organic solvents.[31] To improve the solubility of pristine fullerenes, we blended C_{60} and C_{70} at an optimized ratio, increasing the configuration entropy, which may have increased the solubility of the fullerene molecules.[42, 43] The XRD patterns in Fig. S1 showed the suppressed crystallization of solution processed FM film, which indicated segregation of C_{60} and C_{70} molecules in the FM film. The increased solubility of fullerenes may slow the crystallization of the FM during solvent

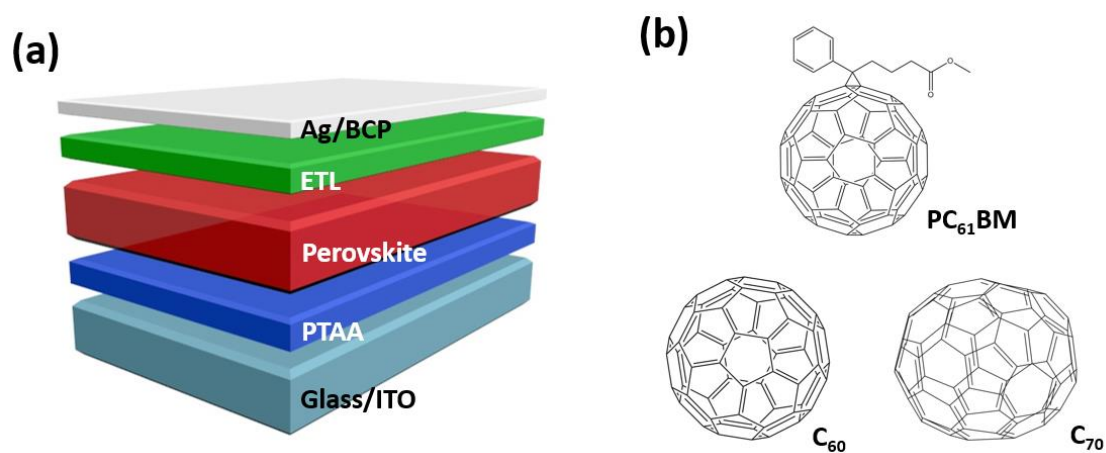removal, allowing the formation of continuous and uniform thin films in the spin-coating process.[25, 26]

Fig. 1. (a) Device construction of the inverted PSCs. (b) Chemical structures of $PC_{61}BM$, C_{60}, and C_{70}.

Table 1 Solubility of C_{60} and C_{70} in three different organic solvents at 25 °C.

Solvent	Chemical structure	Boiling point (°C)	Solute	Solubility at 25 °C (g L^{-1})
Toluene		11	C_{60}	2.1 ± 0.6
			C_{70}	1.2 ± 0.7
CB		131	C_{60}	5.8 ± 0.4
			C_{70}	2.4 ± 0.6
o-DCB		180	C_{60}	22.5 ± 0.9
			C_{70}	27.6 ± 1.2

To determine the optimal ratio of C_{60}:C_{70}, a suitable organic solvent should be selected.

As shown in Table 1, toluene, CB, and o-DCB were chosen to examine the C_{60} and C_{70}

10

solubility, because they are the most widely used solvents for ETL processing.[44-48] The solubilities of C_{60} and C_{70} were the highest in *o*-DCB (22.5 and 27.6 g L^{-1}, respectively), as shown in Table 1. The solubilities of C_{60} and C_{70} in toluene were 2.1 and 1.2 g L^{-1}, respectively, which are similar to those in CB (5.8 and 2.4 g L^{-1}, respectively). In previous studies, the concentration of the PCBM (PC$_{61}$BM or PC$_{71}$BM) solution for ETL preparation was approximately 20–30 g L^{-1}, which ensured a suitable spin-coating speed to obtain a fully covered, uniform film with the appropriate thickness.[30] Therefore, we concluded that of the three organic solvents tested, *o*-DCB was the best candidate for the ETL preparation.

To determine the optimal mixing ratio, we used C_{60} and C_{70} mixtures with different C_{60}:C_{70} ratios (ranging from 0:1 to 1:0) for preparing the FMs. Hereinafter, FM (*a:b*) refers to the mixture of C_{60} and C_{70} at a ratio of *a:b*. As shown in Fig. S2, with the increase of the C_{60} proportion, the solubility of the FMs gradually increased and then decreased after reaching the maximum value (52.9 g L^{-1}) at weight ratio of 1:1. This value is significantly increased compared with those of pristine C_{60} and C_{70} and allows a high spin-coating speed ($\geqslant$2000 rpm), which is essential for uniform film formation. The obtained result corresponds to the condition for the maximum configuration entropy, which is given by the following equation:[30]

$$\Delta S \propto \varphi_{C60} \cdot \varphi_{C70}, \tag{1}$$

where φ_{C60}, φ_{C70}, and S represent the volume fractions of C_{60} and C_{70} and the entropy of the mixture, respectively.

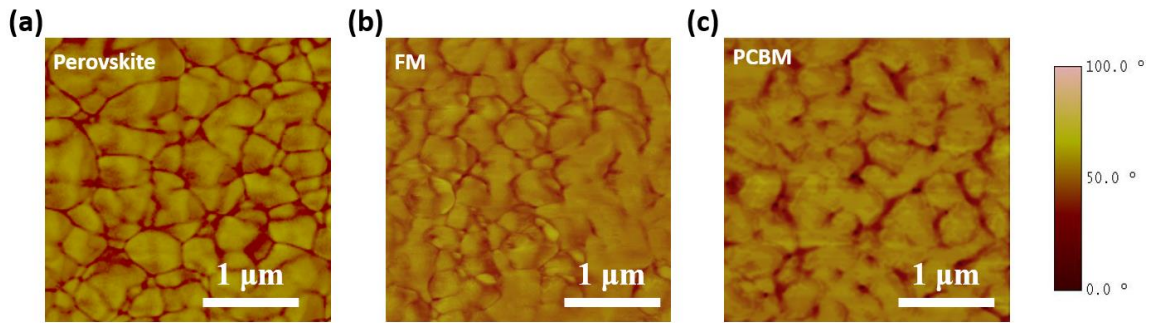Fig. 2. Tapping-mode AFM phase images of (a) the $Cs_{0.05}MA_{0.95}PbI_3$ perovskite film on the ITO/PTAA substrate, (b) the FM film (with a $C_{60}:C_{70}$ ratio of 1:1) on the perovskite film, and (c) the $PC_{61}BM$ layer on the perovskite film.

Fig. 2a shows the AFM images used for investigating the surface morphology of the $Cs_{0.05}MA_{0.95}PbI_3$ perovskite film, which contained perovskite grains with an average diameter of approximately 600 nm. This matches the SEM results shown in Fig. S3. After coating of FM (1:1) onto the perovskite layer, phase distribution of the film showed a more uniform morphology than the $PC_{61}BM$ layer (Fig 2b and c). As shown in Fig. S4a and b, the root-mean-square (RMS) roughness of FM layer was 7.5 nm, lower than that (8.2 nm) of the $PC_{61}BM$ film. We also investigated the surface morphologies of pure C_{60} and C_{70} films on the perovskite layer (Fig. S4c and d). The RMS roughness (obtained from the related AFM height images) of the C_{60} and C_{70} films were 10.2 and 9.8 nm, respectively, indicating that the film uniformity was poorer than that of FM (1:1). The FM (1:1) layer exhibited the most uniform surface, which ensured a good interface connection with the perovskite and cathode.[23]
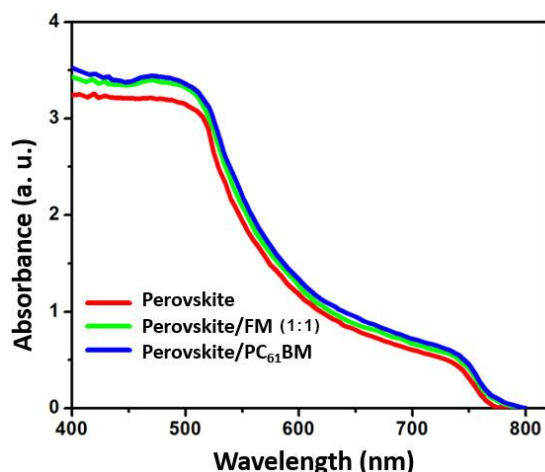
Fig. 3. UV–vis absorption spectra of $Cs_{0.05}MA_{0.95}PbI_3$, $Cs_{0.05}MA_{0.95}PbI_3$/FM (1:1), and

$Cs_{0.05}MA_{0.95}PbI_3$/PC$_{61}$BM films.

To examine the characteristics of the film made of the FM and PC$_{61}$BM, the UV–vis

absorption spectra of $Cs_{0.05}MA_{0.95}PbI_3$ perovskite, $Cs_{0.05}MA_{0.95}PbI_3$/FM (1:1), and

$Cs_{0.05}MA_{0.95}PbI_3$/PC$_{61}$BM films were recorded. As shown in Fig. 3, the absorption was

similar between $Cs_{0.05}MA_{0.95}PbI_3$/FM (1:1) and $Cs_{0.05}MA_{0.95}PbI_3$/PC$_{61}$BM, and these

materials exhibited higher absorption than the pristine perovskite because of the

additional absorption by the FM (1:1) or PC$_{61}$BM. The cross-sectional SEM image in

Fig. 4a shows the dense interfacial connection and the suitable thickness of each layer

(400 and 80 nm for perovskite and ETL, respectively). As shown in Fig. S5, we

investigated the PCE of PSCs employing FM ETLs processed with different blending

ratios. The PSCs using ETLs processed with C_{60}:C_{70} ratios of 1:9, 3:7, 1:1, 7:3, and 9:1

exhibited PCEs of 14.3%, 16.2%, 16.9%, 15.9%, and 14.0%, respectively. As discussed

previously, the fullerene density in the initial ETL solution was 30.0 mg mL^{-1}; because

13

the fullerene solubilities for the FM (9:1) and C_{60} ETLs were lower than this value, as shown in Fig. S2, precipitates formed in the solution and were filtered out. We carefully tuned the spin-coating speed to obtain the same ETL thickness for each blending ratio. The highest PCE (16.9%) was obtained for the 1:1 blending ratio, at which the highest fullerene solubility (52.9 g L^{-1}) was obtained, as shown in Fig. S2. This is consistent with the smooth surface morphology of FM (1:1), which may lead to good carrier transport in the film.[49-51] Although the 1:1 ratio of C_{60} to C_{70} yielded the highest PCE, even 10% addition of C_{70} to C_{60} molecules, which corresponds to FM (9:1), improved the PCE from 13.8% to 14.0%. This contradicts a previous study, in which the PCE of an inverted device was degraded from 15.8% to 15.2% when C_{60} was replaced with FM (9:1). The optimized PCE of the inverted structure in our study, i.e., 16.9%, was achieved by using FM (1:1), whereas in the previous study, the highest PCE (15.8%) was obtained using a C_{60} ETL.[39] This discrepancy might originate from the different experimental conditions between the two studies; for example, the fullerene molecule concentration in the solvent for the ETL film in our experiments was 30 g L^{-1}, except for some cases with low solubilities, whereas that in the previous study was 20 g L^{-1}. Fig. 4b and Table 2 (obtained from forward scans) provide additional details regarding the FM (1:1)-based PSC, which had the open-circuit voltage (V_{oc}) of 1.02 V, J_{sc} of 22.6 mA cm^{-2}, and FF of 73.2%. In comparison, a $PC_{61}BM$-based PSC exhibited a lower PCE of 15.2%, a lower J_{sc} (20.3 mA cm^{-2}), and a lower FF (71.2%). The PSCs employing pure C_{60} and C_{70} as the ETL exhibited even lower PCEs—13.8% and 13.9%,

14

respectively—as shown in Fig. S6. As indicated by the IPCE spectra in Fig. 4c, the integrated J_{sc} for the FM (1:1)- and $PC_{61}BM$-based PSCs were 21.7 and 19.7 mA cm^{-2}, respectively. These values differ by only 2.9%–3.9% from those of the J–V curve in Fig. 4b. The higher IPCE improvement in 650–750 nm range might be caused by the improved charge dissociation of the PSCs using FM as ETL. The V_{oc} of the FM (1:1)-based PSC was 1.02 V, which is lower than that of the $PC_{61}BM$-based PSC (1.05 V), possibly because of the difference in energy levels.[24, 32] V_{oc} can be significantly affected by the lowest unoccupied molecular orbital (LUMO) level of the ETL and the highest occupied molecular orbital level of the HTL.[49] The UPS spectra in Fig. S7a showed that all the C_{60}, C_{70} and FM films exhibited similar energy levels (more details were shown in Table S1). As shown in Fig. S7b, the LUMO of pristine fullerene was approximately −4.3 eV, which is lower than that of $PC_{61}BM$ (−3.8 eV), which may have led to the lower obtained V_{oc}.[32] To examine the photovoltaic efficiency in a steady state, we investigated the maximum steady-state power and photocurrent output, as shown in Fig. 4d. The FM (1:1)-based PSC exhibited a maximum steady-state power and photocurrent output of 16.6% and 22.1 mA cm^{-2}, respectively, which are close to the values in Fig. 4b. The $PC_{61}BM$-based PSC exhibited a maximum steady-state power and photocurrent output of 14.9% and 19.9 mA cm^{-2}, respectively. These results indicate that the ETL made of FM (1:1) had a steady electron-extraction property. The small difference in the values between the J–V characteristics and the maximum steady-state power output may indicate the low hysteresis of the PSCs.[25] The histograms of the

PSCs based on $PC_{61}BM$ and FM (1:1) exhibit a distribution of the PCE, as shown in Fig. S8. More than 70% of the FM (1:1)-based samples exhibited PCEs of >16.5%, indicating the good reproducibility of our results.[50, 51]
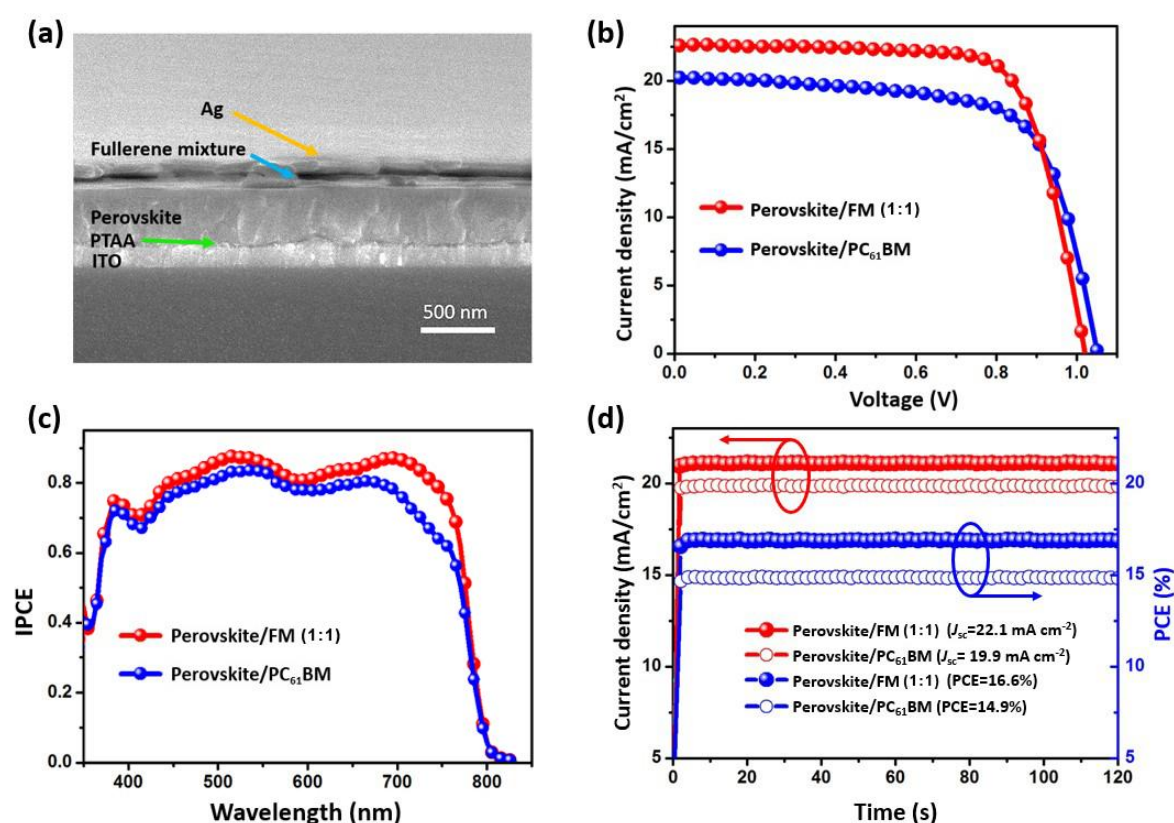

Fig. 4. (a) Cross-sectional SEM image of the PSC using FM (1:1) as the ETL. (b) *J–V* characteristics and (c) IPCE spectra of the PSCs using $PC_{61}BM$ and FM (1:1) as the ETL. (d) Maximum stabilized photocurrent and PCE outputs of the PSCs using FM (1:1) and $PC_{61}BM$ as the ETL.

Table 2 Photovoltaic parameters of PSCs (average values of 20 samples in each group) with various ETLs.

ETL	V_{oc} (V)	J_{sc} (mA cm^{-2})	FF (%)	PCE (%)
PC$_{61}$BM	1.05 ± 0.01	20.3 ± 0.3	71.2 ± 0.7	15.2 ± 0.6
FM (1:1)	1.02 ± 0.01	22.6 ± 0.4	73.2 ± 0.9	16.9 ± 0.7
C$_{60}$	1.01 ± 0.01	19.6 ± 0.3	69.5 ± 0.8	13.8 ± 0.7
C$_{70}$	1.01 ± 0.01	19.8 ± 0.3	70.2 ± 0.8	13.9 ± 0.7

To investigate the superior electron-extraction property of the FM-based ETL, we measured the PL and TRPL spectra of samples with bare perovskite, PC$_{61}$BM/perovskite, and FM (1:1)/perovskite layers. As shown in Fig. 5a, an obvious quenching effect was observed for the PC$_{61}$BM and FM (1:1)-containing films at the wavelength of 770 nm, confirming the excellent electron extraction and transport properties.[52] The quenching effect (quenched by 89.8%) of the FM (1:1)-containing film was larger than that of the PC$_{61}$BM-based film (79.6%), indicating that the ETL made of FM (1:1) had a better electron-extraction property than the ETL made of PC$_{61}$BM.[37] The C$_{60}$ or C$_{70}$ molecule can accommodate several electrons simultaneously, which contributes to the good electron-transport property of pristine fullerene.[53] The biexponential fitted TRPL spectra in Fig. 5b indicate that the PL lifetime values for glass/perovskite/FM (1:1) and glass/perovskite/PC$_{61}$BM were 148 and 172 ns, respectively. The PL lifetime of glass/perovskite/FM (1:1) is 16.2% shorter than that of glass/perovskite/PC$_{61}$BM. These results suggest that the introduction of the FM (1:1)

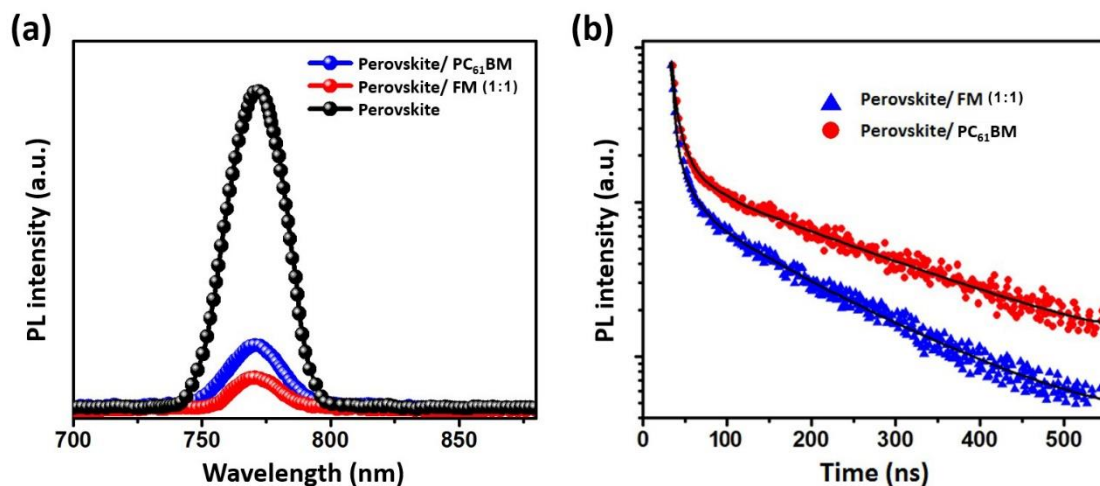layer yielded faster electron extraction, which can suppress the charge-carrier recombination and improve the PCE of PSCs.[33]

Fig. 5. (a) PL spectra of devices with bare perovskite, perovskite/PC$_{61}$BM, and perovskite/FM (1:1) layers. (b) TRPL spectra of devices with glass/perovskite/FM (1:1) and glass/perovskite/ PC$_{61}$BM configurations.

It is also essential to evaluate the interfacial effect and the internal electrical characteristics of the ETL for understanding the advantages of the FM film. Therefore, we performed EIS on FM (1:1)- and PC$_{61}$BM-based PSCs under dark conditions. The Nyquist plots for the PSCs at an applied voltage of 1 V are shown in Fig. 6a. The semicircles can be fitted using a simple equivalent circuit in which R_s represents the internal series resistance, which is related to the connected functional layers of the device, and R_{ct} indicates the charge-transfer resistance, which is related to the process of charge transfer from one layer to another.[51] The R_s (7.31 Ω cm^2) of the FM (1:1)-based PSC is smaller than that of the PC$_{61}$BM-based PSC (9.25 Ω cm^2), which agrees

with the high electron conductivity of pristine fullerene. The R_{ct} of the FM (1:1)-based

PSC is 1202 Ω cm^2, which is approximately 90% higher than that of the PC$_{61}$BM-based

PSC (633 Ω cm^2). The higher R_{ct} can be explained by the superior electron-extraction

property of the interface between the perovskite layer and the ETL, which is beneficial

for transferring electrons to the cathode and preventing charge recombination.[53] We

also measured the J–V characteristics of electron-only devices with the configuration

of ITO/Al/PC$_{61}$BM [or FM (1:1)]/Al to investigate the electron-transport properties of

the ETL. In the high-voltage region, assuming ohmic contact and trap-free transport,

the electron mobility based on the SCLC can be calculated using Mott–Gurney's

equation:[54]

$$J = \frac{9}{8}\varepsilon_r\varepsilon_0\mu\frac{V^2}{L^3} \tag{2}$$

where ε_r, ε_0, μ, and L represent the dielectric constant of fullerene, permittivity of free

space, electron mobility, and thickness of the active layer, respectively.[55] As shown in

Fig. S9, the calculated electron mobility of FM (1:1) was approximately 3×10^{-3} cm^2

v^{-1} s^{-1}, whereas the PC$_{61}$BM-based device exhibited an electron mobility of only 6×10^{-4} cm^2 v^{-1} s^{-1}. The electron mobility of PC$_{61}$BM is approximately 80% lower than that of

FM (1:1), in good agreement with R_s obtained from the EIS measurements, indicating

that the electron transport was better in FM (1:1) than in PC$_{61}$BM. As shown in Fig. 6b,

the dark J of the FM (1:1)-based PSCs under the reverse bias was lower than that of the

PC$_{61}$BM-based devices, indicating that the leakage current of the PSCs was reduced by

replacing PC$_{61}$BM with the FM as the ETL.[50] Because the leakage current is related to

the carrier recombination, the reduced leakage current for the FM (1:1)-based devices may indicate that the ETL made of FM (1:1) had an excellent electron-extraction property.[44] Furthermore, in the forward bias region (from 0.5 to 1.0 V), the PSCs with FM (1:1) as the ETL exhibited a higher injected J than the $PC_{61}BM$-based PSCs, indicating a reduced injection barrier.[50] This can be explained by the high electron mobility of pristine fullerene, which allows electrons to be effectively extracted from perovskite and transferred to the cathode.[53]
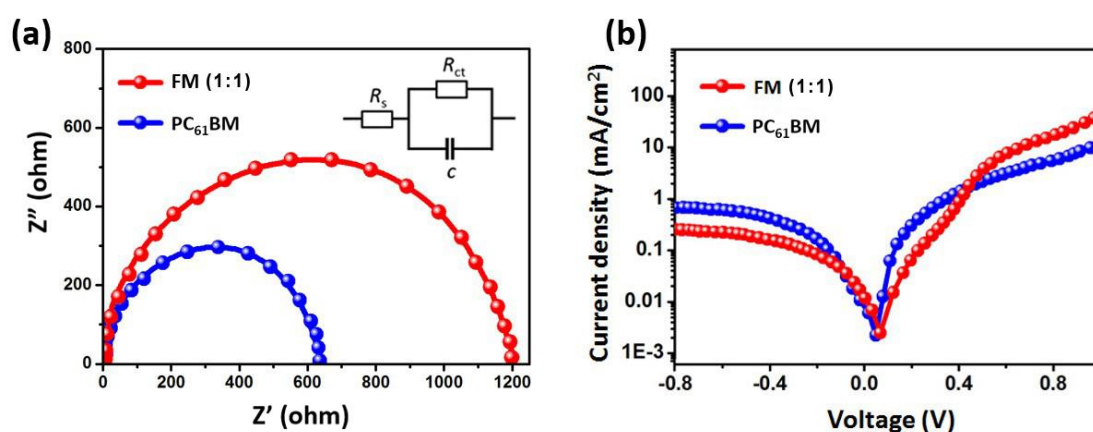

Fig. 6. (a) Nyquist plots of PSCs using FM (1:1) and $PC_{61}BM$ as the ETL, measured in the dark. (b) Logarithmic plots of the dark J–V characteristics of PSCs using FM (1:1) and $PC_{61}BM$ as the ETL.
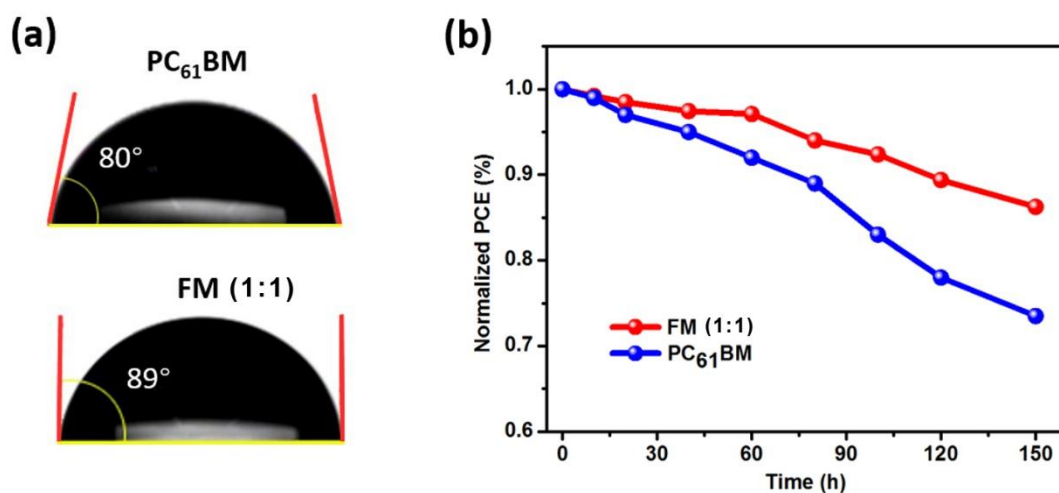
Fig. 7. (a) Contact-angle images of a water droplet on $PC_{61}BM$ and FM (1:1) films. (b) Variation of the normalized PCE with respect to time for PSCs using $PC_{61}BM$ and FM (1:1) as the ETL in air, without encapsulation.

The long-term stability of PSCs with FM (1:1) and $PC_{61}BM$ as the ETL was assessed under ambient conditions (45% humidity and 25 °C, without encapsulation). Environmental humidity is a crucial factor causing the degradation of PSCs.[49, 56] As shown in Fig. 7a, the water contact angles of $PC_{61}BM$ and FM (1:1) films are 80° and 89°, indicating that the FM (1:1) film is more hydrophobic than the $PC_{61}BM$ film. The higher hydrophobicity of the FM (1:1) film may provide higher moisture tolerance for the device and thus enhance the long-term stability compared with PSCs employing $PC_{61}BM$ as the ETL.[22, 23] Consequently, the PSC with FM (1:1) as the ETL retained >85% of their original PCE (16.9%) after 150 h, as shown in Fig. 7b, whereas the PSC with $PC_{61}BM$ as the ETL only maintained ~74% of its initial PCE (15.2%). The results

indicate that the FM (1:1) layer provided robust moisture tolerance, protecting the PSCs from degradation caused by moisture.

Conclusions

We used a mixture of C_{60} and C_{70} as the ETL in the PSC fabrication process, which led to improvements in the PCE and long-term stability of the PSCs. The solubility of the C_{60} and C_{70} mixture in o-DCB was greatly enhanced to 52.9 g L^{-1} at an optimal ratio of 1:1, which was approximately 2.5 times that of a C_{60} solution (22 g L^{-1}). The improved solubility endowed the solution-processed ETL with a homogenous morphology. By employing FM (1:1) as an ETL, the PCE of the PSCs was improved to 16.9%, which was 11.2% higher than that of $PC_{61}BM$-based PSCs (15.2%). PL, EIS, and dark-current analyses indicated the superior electron-extraction property of FM (1:1). These results agreed well with the improvements in the FF and J_{sc}, which are the dominant factors for PCE improvement. Furthermore, the hydrophobic property of the FM (1:1)-based ETL provided excellent moisture protection for the perovskite film, ensuring better long-term stability under ambient conditions. As a result, the FM (1:1)-based PSCs retained approximately 85% of their initial PCE after 150 h of storage under ambient conditions, which was 14.9% higher than that of the $PC_{61}BM$-based PSCs. Our results indicate that employing pristine FM (1:1) as the ETL for PSC fabrication is a simple and cost-effective method for realizing high-efficiency PSCs with long-term stability.

Conflicts of interest

There are no conflicts to declare.

Acknowledgements

Notes and references

1   A. Kojima, K. Teshima, Y. Shirai and T. Miyasaka, *J. Am. Chem. Soc.*, 2009, **131**, 6050-6051.

2   W. S. Yang, B.-W. Park, E. H. Jung, N. J. Jeon, Y. C. Kim, D. U. Lee, S. S. Shin, J. Seo, E. K. Kim and J. H. Noh, *Science*, 2017, **356**, 1376-1379.

3   Q. Jiang, L. Zhang, H. Wang, X. Yang, J. Meng, H. Liu, Z. Yin, J. Wu, X. Zhang and J. You, *Nat. Energy*, 2017, **2**, 16177.

4   M. Saliba, T. Matsui, K. Domanski, J.-Y. Seo, A. Ummadisingu, S. M. Zakeeruddin, J.-P. Correa-Baena, W. R. Tress, A. Abate and A. Hagfeldt, *Science*, 2016, **354**, 206-209.

5   M. M. Lee, J. Teuscher, T. Miyasaka, T. N. Murakami and H. J. Snaith, *Science*, 2012, 1228604.

6   G. Xing, N. Mathews, S. Sun, S. S. Lim, Y. M. Lam, M. Grätzel, S. Mhaisalkar and T. C. Sum, *Science*, 2013, **342**, 344-347.

7   S. D. Stranks, G. E. Eperon, G. Grancini, C. Menelaou, M. J. Alcocer, T. Leijtens, L. M. Herz, A. Petrozza and H. J. Snaith, *Science*, 2013, **342**, 341-344.

8   Y. Liu, Z. Liu and E.-C. Lee, *ACS Appl. Energy Mater.*, 2019, **2**, 1932-1942.

9   G. Liu, X. Xie, F. Zeng and Z. Liu, Energy Technology, 2018, **6**, 1283-1289.

10   L. Chen, X. Xie, Z. Liu and E.-C. Lee, *J. Mater. Chem. A*, 2017, **5**, 6974-6980.

11   Y. Liu, Z. Liu and E.-C. Lee, *J. Mater. Chem. C*, 2018, **6**, 6705-6713.

12   Y. Hu, T. Qiu, F. Bai, X. Miao and S. Zhang, *J. Mater. Chem. A*, 2017, **5**, 25258-25265.

13 H. Zhou, Q. Chen, G. Li, S. Luo, T.-b. Song, H.-S. Duan, Z. Hong, J. You, Y. Liu and Y. Yang, *Science*, 2014, **345**, 542-546.

14 N. J. Jeon, J. H. Noh, W. S. Yang, Y. C. Kim, S. Ryu, J. Seo and S. I. Seok, *Nature*, 2015, **517**, 476.

15 A. Mei, X. Li, L. Liu, Z. Ku, T. Liu, Y. Rong, M. Xu, M. Hu, J. Chen and Y. Yang, *Science*, 2014, **345**, 295-298.

16 M. He, D. Zheng, M. Wang, C. Lin and Z. Lin, *J. Mater. Chem. A*, 2014, **2**, 5994-6003.

17 M. A. Green, A. Ho-Baillie and H. J. Snaith, *Nature photon.*, 2014, **8**, 506. X. Xie, G. Liu, G. Cheng, Z. Liu and E.-C. Lee, *J. Mater. Chem. C*, 2018, **6**, 2793-2800.

18 C. Xu, Z. Liu and E.-C. Lee, *J. Mater. Chem. C*, 2018, **6**, 6975-6981.

19 Z. Liu, X. Xie, G. Liu and E.-C. Lee, *Org. Electron.*, 2019, **64**, 195-201.

20 X. Xie, G. Liu, G. Cheng, Z. Liu and E.-C. Lee, *J. Mater. Chem. C*, 2018, **6**, 2793-2800.

21 M. Hu, C. Bi, Y. Yuan, Y. Bai and J. Huang, *Adv. Sci. (Weinh)*, 2016, **3**, 1500301.

22 C. Bi, Q. Wang, Y. Shao, Y. Yuan, Z. Xiao and J. Huang, *Nat. Commun.*, 2015, **6**, 7747.

23 C. Xu, Z. Liu and E.-C. Lee, *J. Mater. Chem. C*, 2018.

24 C. M. Wolff, F. Zu, A. Paulke, L. P. Toro, N. Koch and D. Neher, *Adv. Mater.*, 2017, **29**.

25 Y. Li, Y. Zhao, Q. Chen, Y. M. Yang, Y. Liu, Z. Hong, Z. Liu, Y. T. Hsieh, L. Meng, Y. Li and Y. Yang, *J. Am. Chem. Soc.*, 2015, **137**, 15540-15547.

26 C.-Y. Chang, W.-K. Huang, Y.-C. Chang, K.-T. Lee and C.-T. Chen, *J. Mater. Chem. A*, 2016, **4**, 640-648.

27 P. H. Wöbkenberg, D. D. Bradley, D. Kronholm, J. C. Hummelen, D. M. de Leeuw, M. Cölle and T. D. Anthopoulos, *Synth. Met.*, 2008, **158**, 468-472.

28 R. C. MacKenzie, J. M. Frost and J. Nelson, *J. Chem. Phys.*, 2010, **132**, 064904.

29 S. Rossbauer, C. Müller and T. D. Anthopoulos, *Adv. Funct. Mater.*, 2014, **24**, 7116-7124.

30 A. D. Mendaza, A. Melianas, S. Rossbauer, O. Backe, L. Nordstierna, P. Erhart, E. Olsson, T. D. Anthopoulos, O. Inganas and C. Muller, *Adv. Mater.*, 2015, **27**, 7325-7331.

31 C. I. Wang and C. C. Hua, *J. Phys. Chem. B*, 2015, **119**, 14496-14504.

32 J. Y. Jeng, Y. F. Chiang, M. H. Lee, S. R. Peng, T. F. Guo, P. Chen and T. C. Wen, *Adv. Mater.*, 2013, **25**, 3727-3732.

33 P.-W. Liang, C.-C. Chueh, S. T. Williams and A. K. Y. Jen, *Adv. Energy Mater.*, 2015, **5**, 1402321.

34 Q. Wang, Y. Shao, Q. Dong, Z. Xiao, Y. Yuan and J. Huang, *Energy Environ. Sci.*, 2014, **7**, 2359-2365.

35 J. Xie, V. Arivazhagan, K. Xiao, K. Yan, Z. Yang, Y. Qiang, P. Hang, G. Li, C. Cui, X. Yu and D. Yang, *J. Mater. Chem. A*, 2018, **6**, 5566-5573.

36   J. You, Z. Hong, Y. M. Yang, Q. Chen, M. Cai, T. B. Song, C. C. Chen, S. Lu, Y. Liu, H. Zhou and Y. Yang, *ACS Nano*, 2014, **8**, 1674-1680.

37   W. Zhang, Y. C. Wang, X. Li, C. Song, L. Wan, K. Usman and J. Fang, *Adv. Sci. (Weinh)*, 2018, **5**, 1800159.

38   A. Anctil, C. W. Babbitt, R. P. Raffaelle and B. J. Landi, *Environ. Sci. technol.*, 2011, **45**, 2353-2359.

39   H. S. Lin, I. Jeon, R. Xiang, S. Seo, J. W. Lee, C. Li, A. Pal, S. Manzhos, M. S. Goorsky, Y. Yang, S. Maruyama and Y. Matsuo, *ACS Appl. Mater. Interfaces*, 2018, **10**, 39590-39598.

40   K. N. Semenov, N. A. Charykov, V. A. Keskinov, A. K. Piartman, A. A. Blokhin and A. A. Kopyrin, *J. Chem. Eng. Data*, 2009, **55**, 13-36.

41   A. D. de Zerio Mendaza, J. Bergqvist, O. Bäcke, C. Lindqvist, R. Kroon, F. Gao, M. R. Andersson, E. Olsson, O. Inganäs and C. Müller, *J. Mater. Chem. A*, 2014, **2**, 14354-14359.

42   G. B. Adams, M. O'Keeffe and R. S. Ruoff, *J. Phys. Chem.*, 1994, **98**, 9465-9469.

43   R. Haselmeier, M. Holz, M. Kappes, R. Michel and D. Fuchs, *Phys. Chem. Chem. Phys.* 1994, **98**, 878-881.

44   Z. Liu and E.-C. Lee, *Org. Electron.*, 2015, **24**, 101-105.

45   N. J. Jeon, J. H. Noh, Y. C. Kim, W. S. Yang, S. Ryu and S. I. Seok, *Nat. Mater.*, 2014, **13**, 897-903.

46   W. Nie, H. Tsai, R. Asadpour, J.-C. Blancon, A. J. Neukirch, G. Gupta, J. J. Crochet, M. Chhowalla, S. Tretiak and M. A. Alam, *Science*, 2015, **347**, 522-525.

47   T. Du, J. Kim, J. Ngiam, S. Xu, P. R. F. Barnes, J. R. Durrant and M. A. McLachlan, *Adv. Funct. Mater.*, 2018, **28**, 1801808.

48   T. Bu, L. Wu, X. Liu, X. Yang, P. Zhou, X. Yu, T. Qin, J. Shi, S. Wang, S. Li, Z. Ku, Y. Peng, F. Huang, Q. Meng, Y.-B. Cheng and J. Zhong, *Adv. Energy Mater.*, 2017, **7**.

49   W. Tress, M. Yavari, K. Domanski, P. Yadav, B. Niesen, J. P. Correa Baena, A. Hagfeldt and M. Graetzel, *Energy Environ. Sci.*, 2018, **11**, 151-165.

50   J. Huang, M. Wang, L. Ding, Z. Yang and K. Zhang, *RSC Adv.*, 2016, **6**, 55720-55725.

51   W. Xu, X. Yao, T. Meng, K. Wang, F. Huang, X. Gong and Y. Cao, *J. Mater. Chem. C*, 2017, **5**, 4190-4197.

52   P. W. Liang, C. Y. Liao, C. C. Chueh, F. Zuo, S. T. Williams, X. K. Xin, J. Lin and A. K. Jen, *Adv. Mater.*, 2014, **26**, 3748-3754.

53   C. D. Weber, C. Bradley and M. C. Lonergan, *J. Mater. Chem. A*, 2014, **2**, 303-307.

54   V. D. Mihailetchi, J. Wildeman and P. W. Blom, *Phys. Rev. Lett.*, 2005, **94**, 126602.

55   G.-W. Kim, D. V. Shinde and T. Park, *RSC Adv.*, 2015, **5**, 99356-99360.

56   T. A. Berhe, W.-N. Su, C.-H. Chen, C.-J. Pan, J.-H. Cheng, H.-M. Chen, M.-C. Tsai, L.-Y. Chen, A. A. Dubale and B.-J. Hwang, *Energy Environ. Sci.*, 2016, **9**, 323-356.